

Four Projects in Astrophysical Magnetohydrodynamics

PI: David C. Collins (Florida State University)

1 Introduction

We are requesting 4.3×10^4 SUs on Stampede 2 for the period beginning June 1, 2022. This allocation will support four projects involving astrophysical magnetic fields and turbulence. The first project (*foregrounds*) examines the polarized signal produced by the interstellar medium, which is in the foreground of our understanding of the distant cosmic microwave background (CMB). The second project (*turbulence*) explores analytical formulae we have developed for isothermal turbulence, which is relevant for many astrophysical processes, among them the formation of stars. The third project (*cores*) examines fractal structures in star forming clouds. The fourth project (*galaxies*) simulates entire galaxies, in order to understand the growth of the magnetic field, and the spatial distribution of magnetic fields for CMB foreground removal. This research is supported by two NSF grants. The first two projects (*turbulence* and *cores*) are supported by NSF AST-1616026, and the third (*foregrounds*) is supported by NSF AST-2009870. We are hopeful that the *galaxies* project will be funded by a pending proposal.

These projects support three graduate students. Luz Jimenez Vela is working on the *cores* project; Branislav Rabatin is working on the *turbulence* and *foregrounds* projects; and Jacob Strack is working on the *galaxies* project.

Table 1 shows the cost for each project in SUs, as well as the disk usage, physics packages, number of simulations to be run, and number of nodes to be used. 64 cores per node will be used for all runs. Also included is the storage need for our existing archive of data, much of which is still generating publications. Two projects are fixed resolution driven turbulence (*turbulence* and *foregrounds*), and two use more expensive gravity and adaptive mesh refinement (*cores* and *galaxies*). In Section 2 we describe the computational tools to be used. We motivate each project and describe the simulations to be run in Section 3. In Section 4 we give the projected cost and disk usage of these simulations.

Table 1: Summary of allocation request. The total node hours and disk usage are in the first two columns, broken down by project. The physics packages used in each project determine the cost and scalability. N_{sim} is the number of simulations in the suite, some of which may run concurrently. N_N , is in the number of nodes to be used. 64 cores per node will be used for all simulations.

Name	Node Hours	Disk	Physics	N_{sim}	N_N
<i>foregrounds</i>	1.5×10^4	9.0×10^3	Driven Turbulence	4	64
<i>turbulence</i>	2.4×10^4	4.8×10^3	Driven Turbulence	5	64
<i>cores</i>	1.0×10^3	2.0×10^4	Gravity+AMR	3	8
<i>galaxies</i>	2.9×10^3	1.1×10^3	Gravity+AMR	2	8
Archive	–	7.0×10^4			
		4.3×10^4		1.1×10^5	

2 Computational Method

For the proposed simulations, we will use Enzo (Bryan et al. 2014; Collins et al. 2010). Enzo is an adaptive mesh refinement (AMR) code, which dynamically adds resolution elements as the simulation evolves. (Magnetohydrodynamics is solved on an Eulerian grid using finite volume techniques. AMR is a technique that dynamically adds resolution elements to the flow as it evolves.

For hydrodynamics we use the piecewise parabolic method (Colella & Woodward 1984), and we use a piecewise linear method for MHD (Li et al. 2008). The AMR uses the scheme of Berger & Colella (1989), and the MHD

uses the scheme of [Balsara \(2001\)](#). Gravity is solved with fast Fourier transforms on the root grid, and multi-grid relaxation on the sub-grid patches ([Bryan et al. 2014](#)).

The *turbulence*, *cores*, and *foregrounds* simulations use an isothermal equation of state. Heating and cooling for the *galaxies* simulations will be handled with the package Grackle ([Smith et al. 2017](#)).

Turbulent driving in the *turbulence* and *foregrounds* simulations will be done by adding a large-scale random velocity field at every time step, with the velocity field evolving using an Ornstein-Uhlenbeck process ([Schmidt et al. 2009](#)).

3 Scientific Background

The common thread among these projects is turbulence. We discuss the aspects of turbulence that apply to all of our projects in Section 3.1. We discuss the relevance of each project and the simulations to be run in the sections that follow. We present the *foregrounds* project in Section 3.2, the *turbulence* project in Section 3.3, the *cores* project in 3.4, and finally the *galaxies* project in 3.5.

3.1 Background: Turbulence Basics

Turbulence underpins all of the projects in this proposal, the first two most notably. Here we describe the aspects of a turbulent system that impact the design of our simulations, the excellent work of [Frisch \(1995\)](#) has more details.

In a turbulent system, energy is injected at a scale, $L_{driving}$. By way of fluid instabilities, the energy cascades to smaller and smaller scales until molecular interactions dissipate the energy at a scale L_{diss} . The energy spectrum behaves like a powerlaw, $E(k) = k^a$. For incompressible fluid turbulence, $a = -5/3$, but that exponent varies with the inclusion of supersonic (compressible) flow and magnetic fields. The region between $L_{driving}$ and L_{diss} , where the powerlaw is valid, is referred to as the *inertial range*. Here, the nonlinear inertial terms in the Navier-Stokes equation dominates over the dissipation terms, and it is the behavior of the nonlinear terms that we wish to explore. $L_{driving}$ is set by the boundary of the simulation. L_{diss} is set by details of the solver and the energy of the flow. Thus, for a given driving energy, the only way to increase the size of the inertial range is with resolution. The inclusion of magnetic fields only shrinks the inertial range and makes the problem harder.

At a resolution of 256^3 , the driving scale and dissipation scale overlap, and there is not much inertial range to work with. At 512^3 , an inertial range appears, but it is small, and determining the actual powerlaw portion of the spectrum is error-prone. This will be demonstrated in Section 3.2. At 1024^3 , a reasonable powerlaw appears even for magnetized simulations. Further increase of the resolution is desirable, but the cost scales like the number of zones on a side to the fourth power, while the size of the inertial range is only linear. Increases in resolution to 2048^3 and beyond is possible and desirable, but also quite costly in terms of total *SU*, disk, and human time. This will be explored if the results of the current proposal indicate it is necessary.

Turbulence is a chaotic process, and must be handled statistically. A single snapshot from a turbulent box is largely random, the true nature must be averaged over a window of time. Additionally, we focus on fully developed turbulence, which takes some simulation time to develop. Thus we run our simulations for a period of time to develop the turbulence, and a period of time for statistical averaging. This is discussed in detail in the next two sections.

For the *foregrounds* and *turbulence* simulations, we will use a resolution of 1024^3 to obtain inertial ranges that are well defined. For the *cores* suite, we will use a root grid of 512^3 to offset the cost of 4 levels of AMR and gravity. The *galaxies* will use a root grid of 256^3 and 8 levels of AMR, and sacrifices well resolved turbulence for spatial dynamic range. Properly resolving the turbulence in the galaxy as well as the circumgalactic media is presently impossible.

Simulation purpose and design will be described further in the next sections.

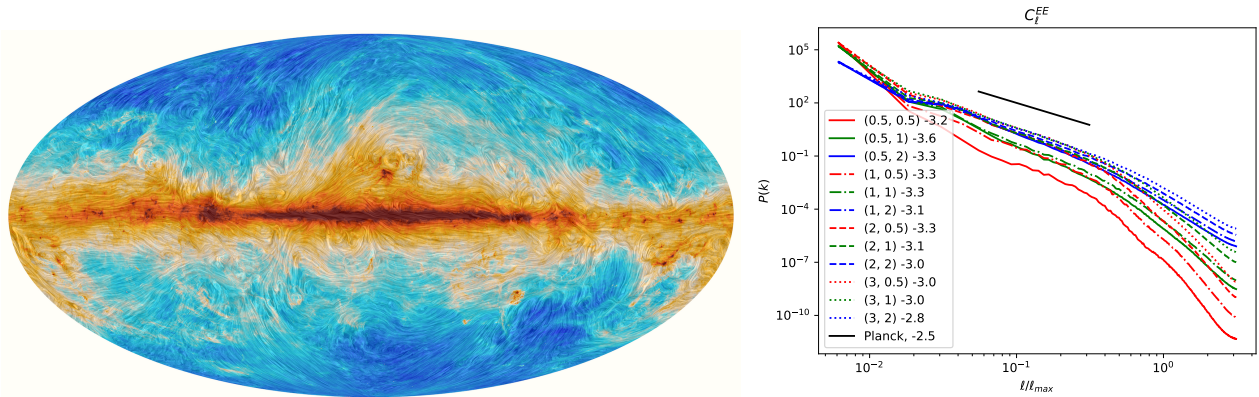


Figure 1: (Left) The large scale magnetic field of the galaxy as seen by the Planck satellite. The color field shows dust emission at 353GHz. The image is smeared along the direction of the magnetic field ([Planck Collaboration et al. 2015](#)). The *foregrounds* project aims to understand the observational properties of this signal, while the *galaxies* project aims to understand its origin. (Right) The power spectrum of the polarization showing E -mode power vs. wavenumber for a preliminary suite of simulations (colored lines) and the galaxy (black line).

3.2 Background: CMB Foregrounds

The cosmic microwave background (CMB) is the light leftover from the creation of the universe. It has taught us a considerable amount about the structure, history, and future of the universe. To learn more from it, we must understand its polarization. To see the polarization of the CMB, we must first understand the polarization of the interstellar medium (ISM), which is much brighter and in the way. This project will perform simulations of driven magnetized turbulence, and compare the structures found on the sky. We will motivate this project in Section 3.2.1, and describe the simulations we will perform in Section 3.2.2

3.2.1 Motivation: *foregrounds*

When the universe was very young, it was very small, and also very hot. So hot that everything was ionized. Sound waves generated by the big bang travel through the universe, causing temperature fluctuations. Once the universe cooled enough, the electrons and protons combined to make the first Hydrogen. After this time, photons can travel great distances without running into an electron. These photons are the CMB. It is an extremely uniform 2.7K black body. Small (μK) fluctuations in this temperature have been studied extensively by satellites such as Planck ([Planck Collaboration et al. 2020](#)). These fluctuations have answered many questions about the content and eventual fate of the universe. But there are still open questions.

Why is the CMB a single temperature? The universe is very large, and one side of the observable universe has never been in contact with the other. Given the expansion of the universe, one would expect significant fluctuations in temperature on the angular size of the full moon on the sky. One possible answer is an extremely rapid *inflation* of the universe, where the universe expands from the size of a proton to the size of the solar system within the first 10^{-16} s. This is different from the *expansion* of the universe, which has been well established and a much more leisurely pace. Such a rapid event would allow different patches of the universe to be at the same temperature very early on. It is also extraordinarily violent, would leave a sea of gravitational waves. These gravitational waves, being quadrupolar in nature, imprint a polarization on the CMB. To detect this polarization is to witness the violent birth of the Universe.

Unfortunately (for observing the CMB) the Galaxy we live in is filled with dust, which gives a polarized signal in the same frequency range as the polarized CMB. This dust, which includes iron and magnesium, lines up per-

pendicular to the magnetic field in the galaxy, not unlike iron filings around a bar magnet. These aligned grains radiate polarized thermal radiation in the microwave and infrared, and so the dust polarization is perpendicular to the magnetic field. This polarized signal is much brighter than the polarization in the CMB, so it must be removed. In order to remove it, we must understand the statistical properties of the turbulent interstellar medium of the Galaxy.

The polarization vector of a photon is given by orientation of its electric field. This is a quantity that depends on the orientation of the camera observing it, which is difficult to use since the camera must point over the whole sky. We define two rotationally invariant quantities, E -mode and B -mode, which are the parity-even and parity-odd versions of the polarization vector. Briefly, E -mode is polarization at either 90 or 45 degrees to filamentary structure, and B -mode is polarization that is at oblique angles to filaments. More details can be found in [Rotti & Huffenberger \(2019\)](#).

The Planck satellite ([Planck Collaboration et al. 2015](#)) measured the galactic polarization, and the result can be seen in Figure 1. The left panel shows the 353 GHz dust emission in color, and the image is smeared along the direction of the magnetic field at every point. The right panel shows the power spectrum of the polarization from simulations (colored lines) and Planck (black line). This plot shows C_ℓ^{EE} , the amplitude in E -mode power, vs wavenumber ℓ . It is found ([Planck Collaboration et al. 2015](#)) that both quantities are distributed over all scales in a power-law fashion, with $E \propto \ell^{-2.5}$. B has a similar exponent but half the amplitude.

The colored lines in Figure 1 are the results of a suite of MHD simulations to be published in Stalpes et al 2022 (in prep). This was a suite of magnetized turbulence simulations at various r.m.s velocities and magnetic field strengths at a resolution of 512^3 performed on *Stampede2*. The simulations were parameterized by the sonic Mach number, $\mathcal{M}_S = v/c_s$, the r.m.s. velocity relative to the speed of sound, c_s ; and the Alfvén Mach number, $\mathcal{M}_A = v/c_A$, the r.m.s velocity relative to the speed of magnetic waves, c_A . These are seen in the legend of the figure, along with the powerlaw exponent of the line. Two things are of note. First, the slopes are all steeper than that found by Planck. And second, most notably the bottom red line, is the poor linear quality of the resulting spectra. These shortcomings are the result of inadequate resolution, as discussed in Section 3.1.

3.2.2 Simulations: foregrounds

Our previous suite of simulations (Stalpes et al 2022, in prep) was run at a resolution of 512^3 , which is insufficient to match the behavior of the sky. The current simulations will double the size of the inertial range by doubling the resolution to 1024^3 , and target parameter space suggested by that parameter suite. In this case more resolution is better without bound, as the sky we are trying to match has an astronomical separation of scales. However, doubling the inertial range increases the cost by a factor of at least 16, so while higher resolution is possible, is is the expense is not warranted at this time.

The turbulence in our simulations is created by way of large scale forcing. Energy is added to the gas at every time step at the largest scale, in a manner that keeps the injection rate constant ([Mac Low 1999](#); [Schmidt et al. 2009](#)). This is continued for 5 dynamical times, $t_{dyn} = L/V$, where L is the size of the pattern and V is the r.m.s. Mach number of the flow. The first $2t_{dyn}$ are used to establish a steady state, as the chaos of the onset of turbulence causes the properties of the gas to fluctuate wildly at the beginning. We then run for an additional $3t_{dyn}$ to build statistics, and average the power spectra over this window. This gives us three statistically independent spectra to average. Again, more is better, three is the minimum to achieve a converged spectrum.

Our results from Stalpes et al (2022) indicated that an r.m.s. Mach number of 5 is necessary to reproduce the observed spectra. We will run a suite of four simulations with $(\mathcal{M}_S, \mathcal{M}_A) = (1,1), (1,5), (5,1), (5,5)$. This will allow us to bracket the ranges of parameters the ISM experiences with a minimum of simulations.

3.3 Background: Turbulent Energy PDFs

Turbulence is ubiquitous in astrophysical processes. We have developed analytic predictions for the distribution of energies in isothermal turbulence, both supersonic and subsonic. These simulations will verify our analytic predictions, and examine if deviations seen in preliminary studies are due to lack of resolution or interesting physics.

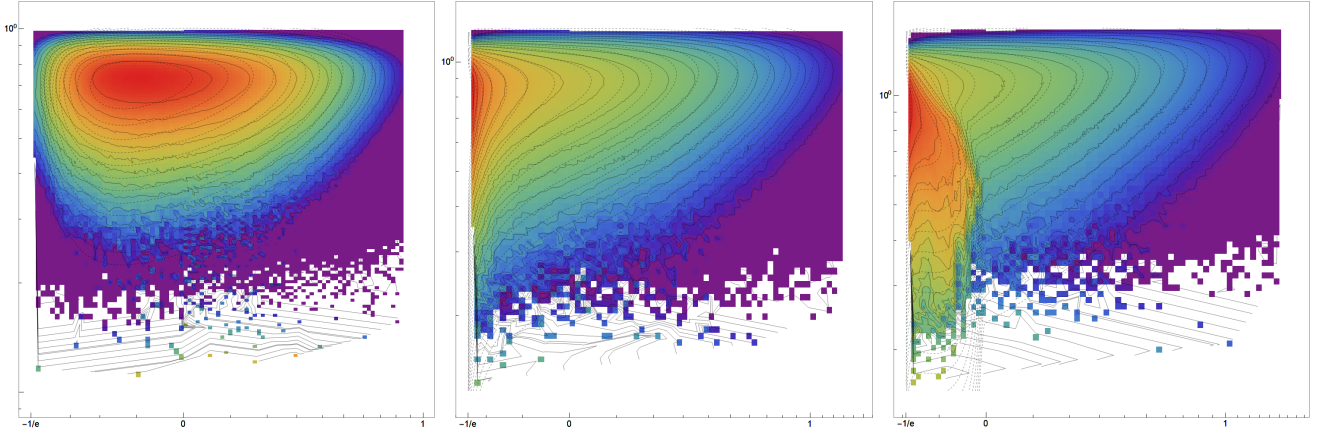


Figure 2: The joint distribution between thermal energy, E_T (horizontal), and kinetic energy E_K (vertical). Color shows the PDF computed from low resolution simulations, and ranges between 0 (purple) and 1 (red). The thermal energy develops a low E_T wall as well as a high E_T wing as the Mach number increases. Dashed lines are our analytic estimate, which is good but has differences that are likely due to resolution.

We provide the background for the *turbulence* project in Section 3.3.1, and motivate the simulations that support this study in Section 3.3.2.

3.3.1 Motivation: *turbulence*

The interstellar medium (ISM) is the gas between stars in the galaxy. It cools very effectively, so can be treated as isothermal (Krumholz 2014). The ISM is also turbulent, with supersonic shocks driven by supernovae causing supersonic turbulence throughout the interstellar medium (Elmegreen & Scalo 2004). This turbulence impacts the formation of stars (see Section 3.4) and causes a polarized screen that is blocking our view of the light from the big bang (see Section 3.2), among many other effects (Elmegreen & Scalo 2004). It is also interesting in its own right. We have developed analytic formulae for the probability density function (PDF) of internal energy and kinetic energy, as well as their joint distribution. In this project we will verify these formulae with high resolution simulations.

Supersonic turbulence is compressible, and the distribution of density fluctuations is described by a log normal, i.e. the log of density is distributed as a Gaussian (Vazquez-Semadeni 1994). The distribution of velocity is roughly Maxwellian, i.e. each of the three velocity components is a Gaussian, and added in quadrature the distribution is Maxwellian. We have recently found analytic distributions for the internal energy and kinetic energy, as well as their joint distribution. (Rabatin et al 2022, in prep). Kinetic energy is defined in the familiar way, $E_K = \frac{1}{2}\rho v^2$. Internal energy is defined as $E_T = c_s^2 \rho \ln \rho / \rho_0$, where c_s is the sound speed and ρ_0 is the mean density (Banerjee & Kritsuk 2018). Figure 2 shows the joint PDF of E_K and E_T for three simulations at increasing Mach number. The color field shows the PDF derived from low-resolution simulations; the solid lines show logarithmically spaced contours of the data; the dashed lines show the theoretical prediction. The first panel is subsonic, with $M_S = 0.5$, the middle has $M_S = 1$, and the third panel is slightly supersonic, with $M_S = 2$. Significant changes in the behavior of the distribution, with high E_K gas developing along side high E_T gas, are both predicted by the analytical dashed lines and seen in the data. This series of figures shows the difficulty of getting gas to large densities, i.e. large values of E_T . Gas with low E_K is found predominantly with low E_T , while at higher kinetic energy the thermal energy distribution becomes more broad, creating higher density gas. This will be useful in understanding, e.g., what gas in a molecular cloud becomes dense enough to form stars.

Our preliminary simulations were run with a modest resolution of 256^3 . This is enough to find reasonable agreement, but imperfect. This can be seen most easily in the first panel of Figure 2, by examining the center most

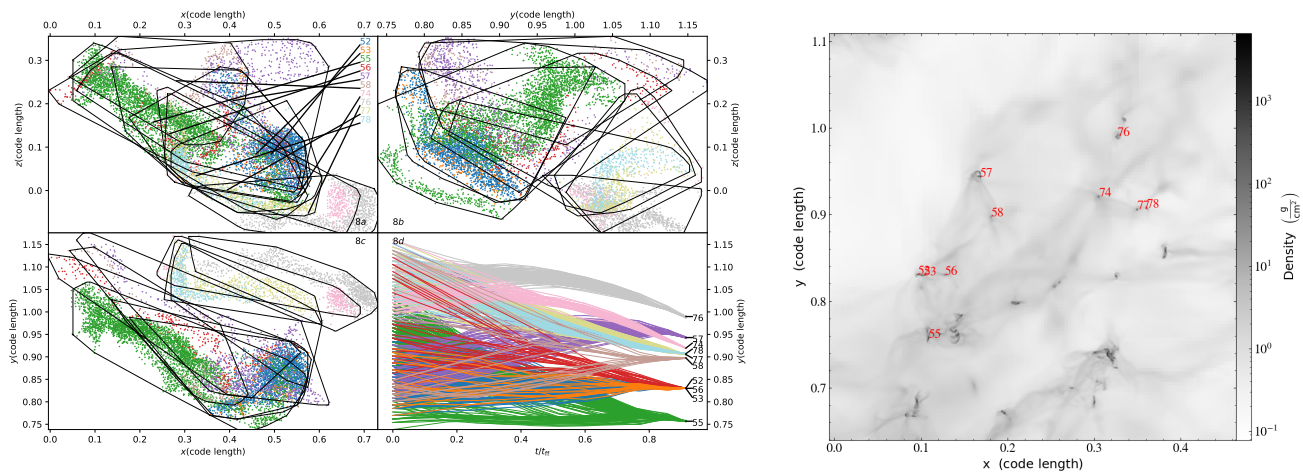


Figure 3: The collapse of several neighboring cores. (Left) The initial positions of the cores along each axis (3a-3c) and the y-coordinate vs. time (3d). (Right) A projection of the domain, showing these cores as well as several others. Different cores begin as fractal objects, intertwined with one another.

(red) contours. The solid line shows simulation, while the dashed line shows theory, which clearly agrees, but only approximately. This lack of agreement can be one of several things, the first to examine is numerical resolution. As discussed in Section 3.2, at low resolution the driving range and dissipation ranges intersect. This causes results that are determined by the numerics, not the nonlinear dynamics of the equations. With insufficient resolution, energy is transferred from large to small scales faster than would be natural, which could be why we have mediocre agreement in our predicted theory.

3.3.2 Simulations: turbulence

The proposed simulations will quadruple this resolution to 1024^3 . As discussed in Section 3.1, this resolution is needed to separate the driving and dissipation ranges. Additionally, the resolution dictates the peak values of density (and other conserved quantities such as E_K and E_T) that the system can attain, as a high density parcel of gas is necessarily small by mass conservation. As discussed above, the benefit of increased resolution is linear in the number of zones across, but the cost scales like the fourth power. If the fits are not improved at 1024^3 , we will propose larger simulations during a future call for proposals.

Turbulence is created in the same manner as the previous CMB simulations (see Section 3.2), wherein large scale energy is added at every time step, and allowed to cascade to small scales. Following the reasoning set out in Section ??, we will run for $5 t_{dyn} = L/V$, where L is the scale of the driving and V is the r.m.s. Mach number. This allows for $2t_{dyn}$ for the establishment of the turbulence, and 3 statistically separate periods to average the PDFs. In both suites of simulations, $5 t_{dyn}$ is the minimum amount of time necessary to achieve meaningful results.

Owing to the substantial evolution in the PDF with Mach number, we will run some subsonic cases ($\mathcal{M}_S=0.5, 1.0$) and some moderate and highly supersonic cases ($\mathcal{M}_S=2, 4, 7$). These are dimensionless physics studies, so the box size and sound speed are unity.

3.4 Background: Star Formation

The formation of stars is filled with filamentary, fractal structures (André et al. 2014). The *cores* project will study the behavior of collapsing gas as it transitions from fractal structures to form dense prestellar cores. We will motivate

the study in Section 3.4.1, and describe the simulations in 3.4.2.

3.4.1 Motivation: *cores*

The formation of stars is one of the most important processes in astrophysics, as stars provide most of the light we see in the night sky, and they produce the energy and metal that dictates the structure and composition of a galaxy. A *prestellar core* is a knot of dense gas formed by gravity in a molecular cloud, which will ultimately form a star. The formation of these cores is one of the more difficult puzzles in star formation, as it is fundamentally dictated by chaotic dynamics of the turbulence in the cloud. This is the focus of the *cores* project.

One of our previous studies (Collins et al 2022, in prep) examined the collapse of a molecular cloud by including semi-Lagrangian tracer particles that follow the flow. The particles that are found in dense cores at the end of the simulation are then followed backwards in time to examine the *preimage* of the gas, before it collapses. This will allow us to better constrain star formation models.

One of the curious findings is the fractal nature of the preimage gas. We find that gas from distinct cores at the end of the simulation begins life mixed with one another in a fractal manner. This can be seen in Figure 3, which shows the overlap of a collection of preimages at the beginning of the simulation in the first 3 panels, and the collapse to form dense cores in the fourth. The length scale in the first three panels translates to roughly 2 pc in size. These panels (3a-3c) show the overlap and fractal, filamentary nature of the gas before it collapses. The last (3d) panel shows the un-mixing of the gas as it collapses in time. The right panel of Figure 3 shows a projection of the prestellar cores at the end of the simulation.

The simulation presented in Figure 3 was one of a suite of three simulations with varied magnetic field strength. We began with fully developed turbulence, and then added tracer particles and turned on gravity and AMR. These simulations were relatively low resolution (128^3 and 4 levels of refinement) as we developed the analysis techniques and learned about extended nature of the primage gas. Our proposed simulations will greatly improve the resolution, to explore if these structures are in fact fractal, or a result of low resolution.

3.4.2 Simulations: *cores*

The proposed simulations will have 512^3 root grid and 4 levels of AMR, and 1024^3 particles. They will also use self-gravity. This resolution strategy is a compromise between a large root grid to resolve the turbulence and deep AMR to capture the cores. A larger root grid would resolve the inertial range more accurately, but the added cost of the AMR overhead and gravity solver makes larger simulations (almost) prohibitively expensive.

The size of the box is 5 pc, and the r.m.s. Mach number is 9. They will begin from existing simulation data.

The proposed suite of three simulations will mirror the magnetic field strengths of the preliminary studies. The simulations will be similar to those presented in (Collins et al. 2012), but with tracer particles and sinks.

The simulations will each run for a total of one free-fall time, where $t_{ff} = (G\rho)^{-1/2} = 1\text{Myr}$ (G is the gravitational constant and ρ is the mean density of the box). Beyond this time, feedback from young stars begins and alters the structure of the cloud, which is beyond the scope of this study.

3.5 Background: Galaxies

The galactic magnetic field can be seen in Figure 1. This figure shows an all-sky projection of dust in the galaxy, as seen by the 353 GHz camera on Planck. The image is smeared along the direction of the magnetic field, which is measured by way of the polarization of the signal. Our goal in the *galaxies* project is to understand the origin of this magnetic field. We will discuss the background in Section 3.5.1, and describe the simulations we will perform in Section 3.5.2

3.5.1 Motivation: *galaxies*

The Milky Way has a large scale magnetic field of roughly $\sim 5\mu\text{G}$, about 200,000 time weaker than a refrigerator magnet, but spanning the entire galaxy. In the previous project, *foregrounds*, the goal is to study the properties of the field with high resolution, while in the *galaxies* project the goal is to study the origin of this field.

The origin of this magnetic field is an open question. There are presently two known *dynamos*, that is mechanisms to amplify magnetic fields. They differ in two ways; the length scales over which they act, and the time scales over which they act. The fast dynamo converts turbulent kinetic energy to magnetic energy at small scales, and produces disordered fields quickly. The slow dynamo produces large scale fields slowly, with large scale convective motions. The magnetic field in the Milky Way, as well as other similar galaxies, shows large scale order, but based on observations of old galaxies, must have been built up quickly.

The proposed simulations will simulate Milky Way sized galaxies and measure the amplification of the magnetic field and process responsible for its amplification, and compare its statistical properties of Galactic fields to those found in the *foregrounds* project.

3.5.2 Simulations: *galaxies*

The disk of our simulated galaxies will be 500pc thick and 25kpc in radius. Our proposed simulation domain will begin at very large scale, 1.3 Mpc. This is to separate the boundary from the region of interest, and to give gas expelled from the galaxies enough volume to expand. This will begin at 256^3 , smaller than the other simulations, but this suite of galaxy simulations has much deeper AMR. We will resolve a nest of refinement grids, each one 1/2 of its parent grid on a side, giving constant number of zones per level. This will be done for 5 levels. We will allow the simulation to refine for a further 3 levels, based on the local density of the gas. Eight levels then gives us 20pc of resolution on the finest level, so we will resolve molecular clouds by a few zones. We will have ample resolution in the disk to study the dynamo action as it occurs, and sufficient resolution in the CGM to serve as an appropriate boundary. As we are simulating the entire galaxy, we can no longer use an idealized isothermal equation of state as the other simulations do, but will use ISM heating and cooling functions by way of the tabulated look up using Grackle (Smith et al. 2017). We will perform two such simulations, one production simulation and one for development. Simulations will last for 1Gyr, four orbital timescales for the galaxy.

These simulations will also be useful in conjunction with the *foregrounds* project. The two approaches compliment each other, as the *foregrounds* simulations will resolve the turbulence with great detail, but the *galaxies* simulations will capture the multiphase nature of the ISM and the large scale morphology.

4 Simulation Plan

Table 2 shows the itemized cost for each suite of simulations, which we discuss in this section.

The wall time for these simulations is found as

$$T_{wall} = \frac{N_Z N_U}{N_C \zeta} \frac{1}{3600} \quad (1)$$

$$\zeta = \frac{\text{zone updates}}{\text{core second}}, \quad (2)$$

where N_Z is the number of zones, N_U is the number of updates, N_C is the total number of cores used, and ζ is the performance of the code given the physics employed. The net cost in SU is then

$$SU = T_{wall} N_N, \quad (3)$$

where N_N is the number of nodes. For all simulations, we will use 64 cores per node, so $N_C = 64N_N$. We will estimate N_Z and N_U from the physics goals in this section. The performance, ζ , is measured in the Scaling document. The number of cores, N_C , is selected from the performance described in the scaling document.

Table 2: Allocation request. Cost for each simulation, SU , is computed from wall time and number of nodes for each suite, per Equations 1, 3. T_{wall} is measured in hours, the number of nodes for each suite can be found in Table 1. The *turbulence* and *foregrounds* suites are itemized by Mach number and Alfvén Mach number, M_s and M_a , which affect the total time, T , and timestep size ΔT . The AMR simulations, *cores* and *galaxies* is are itemized for a single simulation by level, ℓ , and the cost is found by estimating the volume fraction, f_ℓ , covered on level and the time step Δt for that level. The *cores* and *galaxies* simulations are repeated 3 and 2 times. Long term disk usage is estimated as N_Z times the number of fields for each simulation. More details are given in the text.

suite	M_s, M_A	N_Z	T	ΔT	N_U	T_{wall}	SU
<i>foregrounds</i>	1,1	1.1×10^9	2.5	4.3×10^{-5}	5.8×10^4	4.2×10^1	2.7×10^3
<i>foregrounds</i>	1,5	1.1×10^9	2.5	1.4×10^{-5}	1.7×10^5	1.3×10^2	8.1×10^3
<i>foregrounds</i>	5,1	1.1×10^9	0.5	1.4×10^{-5}	3.5×10^4	2.5×10^1	1.6×10^3
<i>foregrounds</i>	5,5	1.1×10^9	0.5	8.7×10^{-6}	5.8×10^4	4.2×10^1	2.7×10^3
						SU	1.5×10^4
						Disk	9.0×10^3
suite	M_s	N_Z	T	ΔT	N_U	T_{wall}	SU
<i>turbulence</i>	0.50	1.1×10^9	5	2.8×10^{-5}	1.8×10^5	1.3×10^2	8.2×10^3
<i>turbulence</i>	1.00	1.1×10^9	2.5	2.1×10^{-5}	1.2×10^5	8.6×10^1	5.5×10^3
<i>turbulence</i>	2.00	1.1×10^9	1.25	1.4×10^{-5}	8.8×10^4	6.4×10^1	4.1×10^3
<i>turbulence</i>	4.00	1.1×10^9	0.625	8.5×10^{-6}	7.3×10^4	5.3×10^1	3.4×10^3
<i>turbulence</i>	7.00	1.1×10^9	0.357	5.3×10^{-6}	6.7×10^4	4.9×10^1	3.1×10^3
						SU	2.4×10^4
						Disk	4800
suite	ℓ	f_ℓ	N_Z	T [Myr]	ΔT	N_U	T_{wall}
<i>cores</i>	0	1	1.3×10^8	1	4.6×10^{-3}	2.2×10^2	6.0×10^{-1}
<i>cores</i>	1	4.6×10^{-1}	5.0×10^8	1	2.3×10^{-3}	4.4×10^2	4.5×10^0
<i>cores</i>	2	8.3×10^{-2}	7.1×10^8	1	1.1×10^{-3}	8.8×10^2	1.3×10^1
<i>cores</i>	3	1.3×10^{-2}	8.7×10^8	1	5.7×10^{-4}	1.8×10^3	3.1×10^1
<i>cores</i>	4	1.8×10^{-3}	10.0×10^8	1	2.9×10^{-4}	3.5×10^3	7.2×10^1
						per sim	1.9×10^3
						SU	5.8×10^3
						Disk	2.0×10^4
suite	ℓ	f_ℓ	N_Z	T [Gyr]	ΔT	N_U	T_{wall}
<i>galaxies</i>	0	1.0×10^0	1.7×10^7	1	3.5×10^{-4}	2.8×10^3	3.2×10^{-2}
<i>galaxies</i>	1	1.0×10^0	1.3×10^8	1	1.8×10^{-4}	5.7×10^3	5.2×10^{-1}
<i>galaxies</i>	2	1.2×10^{-1}	1.3×10^8	1	8.8×10^{-5}	1.1×10^4	1.0×10^0
<i>galaxies</i>	3	2.9×10^{-2}	2.5×10^8	1	4.4×10^{-5}	2.3×10^4	3.9×10^0
<i>galaxies</i>	4	4.2×10^{-3}	2.9×10^8	1	2.2×10^{-5}	4.5×10^4	8.8×10^0
<i>galaxies</i>	5	3.9×10^{-4}	2.2×10^8	1	1.1×10^{-5}	9.1×10^4	1.3×10^1
<i>galaxies</i>	6	3.9×10^{-5}	1.7×10^8	1	5.5×10^{-6}	1.8×10^5	2.1×10^1
<i>galaxies</i>	7	3.9×10^{-6}	1.4×10^8	1	2.8×10^{-6}	3.6×10^5	3.4×10^1
<i>galaxies</i>	8	3.9×10^{-7}	1.1×10^8	1	1.4×10^{-6}	7.3×10^5	5.5×10^1
						SU per sim	8.8×10^3
						SU	1.8×10^4
						Disk	1.0×10^4
						SU	6.3×10^4
						Disk	4.4×10^4

The estimate of the number of zones, N_Z , is determined by the target resolution for the simulation and the expected AMR structure. For the fixed resolution simulations, this is trivial. For the AMR simulations, the actual number of zones is dynamically determined by the portion of the flow that is turning into stars. This is a chaotic process, so formally impossible to predict. However, it can be expected to be roughly similar to previous simulations, so we estimate the covering fraction from those. We measure the covering fraction, f_ℓ , of AMR grids on each level, ℓ , from prior simulations, and compute the number of zones on each level as

$$N_Z = \frac{V f_\ell}{\Delta x_\ell^3}, \quad (4)$$

where V is the total volume for each simulation, and Δx_ℓ on each level is 1/8th that of its parent.

The number of updates, N_U , is found as $N_U = T/\Delta T$, where the total simulation time is T and the size of the timestep is ΔT . T is determined by the physics problem. The size of the time step ΔT is determined by a standard Courant condition, that is a wave cannot cross half of one zone in a timestep,

$$\Delta T = \eta \frac{\Delta x}{v_{\text{signal}}}, \quad (5)$$

and the safety factor $\eta = 0.5$. We determine $v_{\text{signal}} = c_s + v_{\max}$ as the sum of the sound speed and the max velocity, from preliminary studies, and then use use Equation 5 to determine the number of steps on each level.

Both the *turbulence* and *foregrounds* simulations are fixed resolution and employ only the random forcing and hydro/MHD solver. Both will be run at 1024^3 . The total time, T , is 5 shock-crossing times, so $T = 5L/\mathcal{M}_s$, where L is the size of the driving pattern. The timestep, ΔT , also decreases with Mach number as Equation 5, and is determined measuring the signal speed v_{signal} from previous fully developed turbulence simulations and rescaling with the Mach number.

The *cores* simulations will have 512^3 root grid zones and 1024^3 particles, as well as 4 levels of AMR. The refinement will be based on the density. It will use the isothermal MHD solver, the gravity solver, and the particle update machinery. The net cost per zone update for this combination of physics solvers and a similar AMR structure to the production simulations is discussed in the Scaling document. We will perform three of these simulations.

The *galaxies* suite will restrict the dynamic AMR to the disk of the galaxy, and use a tower of refinement, with each level 1/2 the length of the parent, to separate the outer part of the CGM at 1.3 Mpc from the small star forming regions in the disk. The first 5 levels will be static nested AMR levels, the final 3 will be dynamic. For each level we approximate that about 10% coverage of the parent level. This is by construction for the first 5, and from experience with similar simulations for the final 3. These simulations will use the MHD solver, the gravity solver, the particle machinery for the star particles. We have performed a preliminary simulation using 5 levels to determine the anticipated signal speed, v_{signal} , to determine the timestep size.

Table 2 shows the breakdown of the total request by simulation. The *turbulence* and *foregrounds* suites are itemized by Mach number, while the *cores* and *galaxies* suites are itemized by AMR level. Shown in that table is the name; the parameter, either Mach number, level, or Sonic and Alfvén Mach numbers; the volume fraction; the number of zones N_Z ; the total simulation time T ; the timestep size ΔT ; the total number of updates N_U ; the wall time T_{wall} in hours; and finally the total SU cost. The table also displays disk usage for these simulations. The *cores* suite will be repeated 3 times, and the *galaxies* will be repeated twice.

The **long term disk storage** requested has two portions; the new simulations, and our archive of simulations that are still bearing fruit. Our existing archive of previous simulations is 7×10^4 Gb. Disk usage for the current request, presented in Table 2, is estimated from the number of zones, N_Z . Each zone stores a number of fields, N_F : 5 for *turbulence*(density, 3 velocity, and energy); 14 for *cores* and *foregrounds*(density, energy, 3 velocity, 3 magnetic fields, 3 electric fields, 3 additional magnetic fields, see [Collins et al. \(2010\)](#)); 24 for the *galaxies* suite (14 for MHD, 10 for additional chemistry fields.) So the total memory is 8 bytes for all of $N_Z \times N_F$ fields. It is listed in Gb in the table.

5 Access to Other Computational Resources

Local Computing Environment The astrophysics group at Florida State University has a small cluster with 300 cores. This machine is useful for testing and debugging, but not large enough for the proposed simulations. Florida State University also maintains a research cluster, but it is also insufficient for this research.

Other supercomputing resources. The PI of the current proposal does not presently have access to other supercomputing resources.

6 Personnel

The PI of this project is Dr. David C. Collins, an Associate Professor in the Florida State University Department of Physics. Dr. Collins has more than fifteen years of experience working using high performance computing platforms for research in computational astrophysics. He is also a lead developer of the code Enzo, which has a long history of simulation success.

Three PhD students will be working on the projects. Luz Jimenez Vela will be responsible for the *cores* project. Branislav Rabatin is responsible for both the *turbulence* and *foregrounds* projects. Jacob Strack is responsible for the *galaxies* project.

References

- André, P., Di Francesco, J., Ward-Thompson, D., Inutsuka, S. I., Pudritz, R. E., & Pineda, J. E. 2014, in Protostars and Planets VI, ed. H. Beuther, R. S. Klessen, C. P. Dullemond, & T. Henning, 27
- Balsara, D. S. 2001, J. Comput. Phys, 174, 614
- Banerjee, S. & Krtsuk, A. G. 2018, Phys. Rev. E, 97, 023107
- Berger, M. J. & Colella, P. 1989, J. Comput. Phys, 82, 64
- Bryan, G. L., Norman, M. L., O’Shea, B. W., Abel, T., Wise, J. H., Turk, M. J., Reynolds, D. R., Collins, D. C., Wang, P., Skillman, S. W., Smith, B., Harkness, R. P., Bordner, J., Kim, J.-h., Kuhlen, M., Xu, H., Goldbaum, N., Hummels, C., Krtsuk, A. G., Tasker, E., Skory, S., Simpson, C. M., Hahn, O., Oishi, J. S., So, G. C., Zhao, F., Cen, R., Li, Y., & Enzo Collaboration. 2014, ApJS, 211, 19
- Colella, P. & Woodward, P. R. 1984, J. Comput. Phys, 54, 174
- Collins, D. C., Krtsuk, A. G., Padoan, P., Li, H., Xu, H., Ustyugov, S. D., & Norman, M. L. 2012, ApJ, 750, 13
- Collins, D. C., Xu, H., Norman, M. L., Li, H., & Li, S. 2010, ApJS, 186, 308
- Elmegreen, B. G. & Scalo, J. 2004, ARA&A, 42, 211
- Frisch, U. 1995, Turbulence. The legacy of A.N. Kolmogorov
- Krumholz, M. R. 2014, Phys. Rep., 539, 49
- Li, S., Li, H., & Cen, R. 2008, ApJS, 174, 1
- Mac Low, M.-M. 1999, ApJ, 524, 169

Planck Collaboration, Ade, P. A. R., Aghanim, N., Alina, D., Alves, M. I. R., Armitage-Caplan, C., Arnaud, M., Arzoumanian, D., Ashdown, M., Atrio-Barandela, F., Aumont, J., Baccigalupi, C., Banday, A. J., Barreiro, R. B., Battaner, E., Benabed, K., Benoit-Lévy, A., Bernard, J. P., Bersanelli, M., Bielewicz, P., Bock, J. J., Bond, J. R., Borrill, J., Bouchet, F. R., Boulanger, F., Bracco, A., Burigana, C., Butler, R. C., Cardoso, J. F., Catalano, A., Chamballu, A., Chary, R. R., Chiang, H. C., Christensen, P. R., Colombi, S., Colombo, L. P. L., Combet, C., Couchot, F., Coulais, A., Crill, B. P., Curto, A., Cuttaia, F., Danese, L., Davies, R. D., Davis, R. J., de Bernardis, P., de Gouveia Dal Pino, E. M., de Rosa, A., de Zotti, G., Delabrouille, J., Désert, F. X., Dickinson, C., Diego, J. M., Donzelli, S., Doré, O., Douspis, M., Dunkley, J., Dupac, X., Efstathiou, G., Enßlin, T. A., Erikson, H. K., Falgarone, E., Ferrière, K., Finelli, F., Forni, O., Frailis, M., Fraisse, A. A., Franceschi, E., Galeotta, S., Ganga, K., Ghosh, T., Giard, M., Giraud-Héraud, Y., González-Nuevo, J., Górski, K. M., Gregorio, A., Gruppuso, A., Guillet, V., Hansen, F. K., Harrison, D. L., Helou, G., Hernández-Monteagudo, C., Hildebrandt, S. R., Hivon, E., Hobson, M., Holmes, W. A., Hornstrup, A., Huffenberger, K. M., Jaffe, A. H., Jaffe, T. R., Jones, W. C., Juvela, M., Keihänen, E., Keskitalo, R., Kisner, T. S., Kneissl, R., Knoche, J., Kunz, M., Kurki-Suonio, H., Lagache, G., Lähteenmäki, A., Lamarre, J. M., Lasenby, A., Lawrence, C. R., Leahy, J. P., Leonardi, R., Levrier, F., Liguori, M., Lilje, P. B., Linden-Vørnle, M., López-Caniego, M., Lubin, P. M., Macías-Pérez, J. F., Maffei, B., Magalhães, A. M., Maino, D., Mandolesi, N., Maris, M., Marshall, D. J., Martin, P. G., Martínez-González, E., Masi, S., Matarrese, S., Mazzotta, P., Melchiorri, A., Mendes, L., Mennella, A., Migliaccio, M., Miville-Deschénes, M. A., Moneti, A., Montier, L., Morgante, G., Mortlock, D., Munshi, D., Murphy, J. A., Naselsky, P., Nati, F., Natoli, P., Netterfield, C. B., Noviello, F., Novikov, D., Novikov, I., Oxborrow, C. A., Pagano, L., Pajot, F., Paladini, R., Paoletti, D., Pasian, F., Pearson, T. J., Perdereau, O., Perotto, L., Perrotta, F., Piacentini, F., Piat, M., Pietrobon, D., Plaszczynski, S., Poidevin, F., Pointecouteau, E., Polenta, G., Popa, L., Pratt, G. W., Prunet, S., Puget, J. L., Rachen, J. P., Reach, W. T., Rebolo, R., Reinecke, M., Remazeilles, M., Renault, C., Ricciardi, S., Riller, T., Ristorcelli, I., Rocha, G., Rosset, C., Roudier, G., Rubiño-Martín, J. A., Rusholme, B., Sandri, M., Savini, G., Scott, D., Spencer, L. D., Stolyarov, V., Stompor, R., Sudiwala, R., Sutton, D., Suur-Uski, A. S., Sygnet, J. F., Tauber, J. A., Terenzi, L., Toffolatti, L., Tomasi, M., Tristram, M., Tucci, M., Umana, G., Valenziano, L., Valiviita, J., Van Tent, B., Vielva, P., Villa, F., Wade, L. A., Wandelt, B. D., Zacchei, A., & Zonca, A. 2015, *A&A*, 576, A104

Planck Collaboration, Aghanim, N., Akrami, Y., Ashdown, M., Aumont, J., Baccigalupi, C., Ballardini, M., Banday, A. J., Barreiro, R. B., Bartolo, N., Basak, S., Battye, R., Benabed, K., Bernard, J. P., Bersanelli, M., Bielewicz, P., Bock, J. J., Bond, J. R., Borrill, J., Bouchet, F. R., Boulanger, F., Bucher, M., Burigana, C., Butler, R. C., Calabrese, E., Cardoso, J. F., Carron, J., Challinor, A., Chiang, H. C., Chluba, J., Colombo, L. P. L., Combet, C., Contreras, D., Crill, B. P., Cuttaia, F., de Bernardis, P., de Zotti, G., Delabrouille, J., Delouis, J. M., Di Valentino, E., Diego, J. M., Doré, O., Douspis, M., Ducout, A., Dupac, X., Dusini, S., Efstathiou, G., Elsner, F., Enßlin, T. A., Erikson, H. K., Fantaye, Y., Farhang, M., Fergusson, J., Fernandez-Cobos, R., Finelli, F., Forastieri, F., Frailis, M., Fraisse, A. A., Franceschi, E., Frolov, A., Galeotta, S., Galli, S., Ganga, K., Génova-Santos, R. T., Gerbino, M., Ghosh, T., González-Nuevo, J., Górski, K. M., Gratton, S., Gruppuso, A., Gudmundsson, J. E., Hamann, J., Handley, W., Hansen, F. K., Herranz, D., Hildebrandt, S. R., Hivon, E., Huang, Z., Jaffe, A. H., Jones, W. C., Karakci, A., Keihänen, E., Keskitalo, R., Kiiveri, K., Kim, J., Kisner, T. S., Knox, L., Krachmalnicoff, N., Kunz, M., Kurki-Suonio, H., Lagache, G., Lamarre, J. M., Lasenby, A., Lattanzi, M., Lawrence, C. R., Le Jeune, M., Lemos, P., Lesgourgues, J., Levrier, F., Lewis, A., Liguori, M., Lilje, P. B., Lilley, M., Lindholm, V., López-Caniego, M., Lubin, P. M., Ma, Y. Z., Macías-Pérez, J. F., Maggio, G., Maino, D., Mandolesi, N., Mangilli, A., Marcos-Caballero, A., Maris, M., Martin, P. G., Martinelli, M., Martínez-González, E., Matarrese, S., Mauri, N., McEwen, J. D., Meinhold, P. R., Melchiorri, A., Mennella, A., Migliaccio, M., Millea, M., Mitra, S., Miville-Deschénes, M. A., Molinari, D., Montier, L., Morgante, G., Moss, A., Natoli, P., Nørgaard-Nielsen, H. U., Pagano, L., Paoletti, D., Partridge, B., Patanchon, G., Peiris, H. V., Perrotta, F., Pettorino, V., Piacentini, F., Polastri, L., Polenta, G., Puget, J. L., Rachen, J. P., Reinecke, M., Remazeilles, M., Renzi, A., Rocha, G., Rosset, C., Roudier, G., Rubiño-Martín, J. A., Ruiz-Granados, B., Salvati, L., Sandri, M., Savelainen, M., Scott, D., Shellard, E. P. S., Sirignano, C., Sirri, G., Spencer, L. D., Sunyaev, R., Suur-Uski, A. S., Tauber, J. A., Tavagnacco, D., Tenti, M.,

Toffolatti, L., Tomasi, M., Trombetti, T., Valenziano, L., Valiviita, J., Van Tent, B., Vibert, L., Vielva, P., Villa, F., Vittorio, N., Wandelt, B. D., Wehus, I. K., White, M., White, S. D. M., Zacchei, A., & Zonca, A. 2020, A&A, 641, A6

Rotti, A. & Huffenberger, K. 2019, J. Cosmology Astropart. Phys., 2019, 045

Schmidt, W., Federrath, C., Hupp, M., Kern, S., & Niemeyer, J. C. 2009, A&A, 494, 127

Smith, B. D., Bryan, G. L., Glover, S. C. O., Goldbaum, N. J., Turk, M. J., Regan, J., Wise, J. H., Schive, H.-Y., Abel, T., Emerick, A., O'Shea, B. W., Anninos, P., Hummels, C. B., & Khochfar, S. 2017, MNRAS, 466, 2217

Vazquez-Semadeni, E. 1994, ApJ, 423, 681